

MOTION DETECTION IN CT IMAGES WITH A NOVEL FAST TECHNIQUE

© 2013 Z. Islami rad*, **, R. Gholipour Peyvandi*, R. Heshmati*

*Nuclear Science and Technology Research Institute

AEOI, P.O. Box: 14155-1339, Tehran, Iran

**Nuclear Engineering and Physics Department, Amir Kabir University

P.O.Box: 15875-4413, Tehran-Iran

Received December 28, 2011; in final form, July 28, 2012

Different factors may influence the image quality of the first generation computed tomography (CT) system (single-source – single-detector) and one of these factors is the object motion. For studying this effect on image quality, an industrial CT system was designed and developed. Several experiments were performed with different axial and rotational motion of a phantom. The quality of reconstructed images was compared by computing the RMSE of each image. Also, in this paper a processing technique is presented that has the potential to detect the object motion during the acquisition process and to correct it by rescanning from motion point. The presented results can be extended to other medical and industrial applications.

DOI: 10.7868/S0032816213030063

1. INTRODUCTION

Patient motion during the data acquisition process results in an inconsistent set of projection data and a degradation of image quality due to motion artifacts. These artifacts appear in the form of distortions and blurring which may result in inaccurate or misleading diagnoses [1–3]. Different methods have been proposed for detecting and correcting for motion during clinical imaging. Sarkar et al. proposed a method in which patient motions are estimated and compensated using a correlation function based on linograms and sinograms of the projection data [4]. Eisner et al. presented motion identification and correction method based on cross-correlation of summed horizontal and vertical profiles of successive projections [5]. Linney and Gregson extended a method in which one can detect and correct organ motion by using opposite rays in fan-beam projection in CT scanner [6].

In references [7–9], the adaptive interference canceller (AIC) approach is used to remove the motion artifacts identified by the spatial overlap correlator. Another technique is based upon a property of the Radon transform, which states that for a given object the integral of projection data is constant for all projection angles. If the object starts deforming during a CT data acquisition process due to organ motion, this integral will not remain constant over time. Using this property, the phases of periodic in cardiac motion can be identified [10, 11].

In this article, we intended to study the effect of axial and rotational phantom motion on obtained sino-

gram and reconstructed image quality using the RMSE quantity and then proposed a method to detect real time motion and correct artifacts due to phantom motion by repeating the imaging process from motion point. The accuracy of this method is verified using simulated phantom and experimental data.

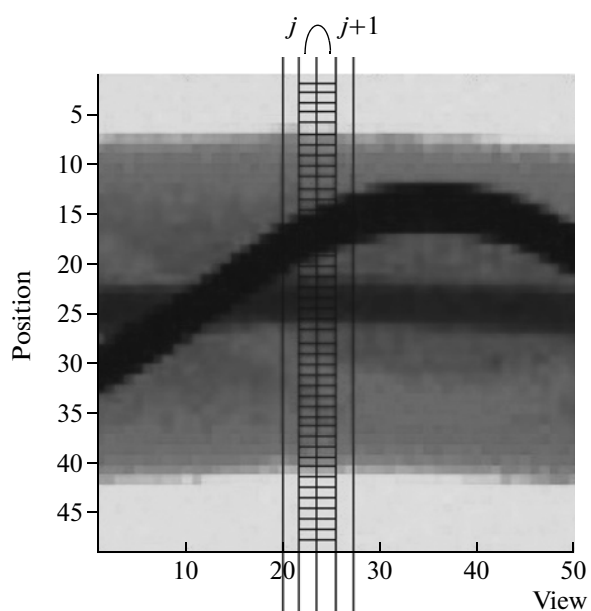


Fig. 1. Selection of two successive view columns ($j + 1$)-th and j -th of sinogram matrix $S(i, j)$.

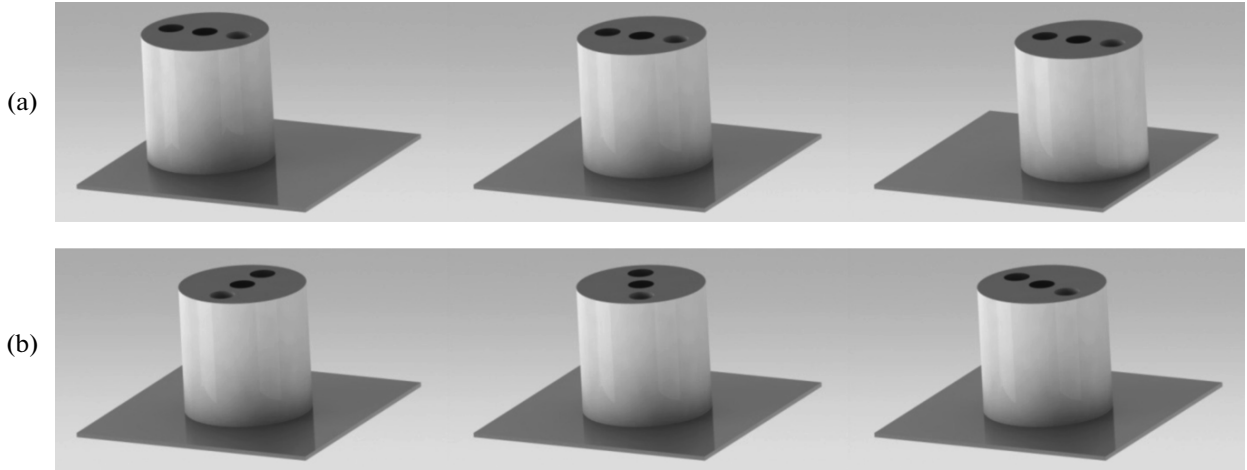


Fig. 2. Phantom displacement for studying of: (a) axial dislocation; (b) rotational dislocation.

2. THEORY

Here, we investigate the effect of axial and rotational motion of phantom on quality of CT images that causes artifacts, which appear as blurring, doubling or streaking, which may lead to an erroneous diagnosis; therefore we proposed a technique to detect phantom motion. The main idea of this technique is to evaluate the continuity of sinogram by subtracting the projection data recorded at two adjacent views. In case of no motion, the results of this subtraction process would be almost zero whereas a nonzero value indicates the presence of motion, so by checking the standard deviation of the difference of sinograms one can observe phantom displacement.

2.1. Radon Transform

Tomography imaging consists of directing γ -rays into an object from multiple orientations and measuring intensity decrease along a series of linear paths. The intensity reduction is characterized by Beer's law, which describes it as a function of γ -ray energy, path length, and linear attenuation coefficient of material [12].

The Radon transform computes projections of an image. The Radon transform can be defined as the collection of projections of an object gathered at various angles. In a γ -ray transmission, the intensity I of a monoenergetic radiation beam traversing a phantom is given by the following equation:

$$g = \ln(I_0/I) = \int_L \mu(x, y) du. \quad (1)$$

Where I_0 is the incident beam intensity of the radiation beam; du is some differential path length; $\mu(x, y)$ is the function describing the two-dimensional distribution of attenuation coefficient in the imaged object at the point (x, y) ; g , the transmittance of the object, is de-

fined as the logarithm of the ratio of the intensity of the detected beam to the intensity of the emitted beam and L is the line along which the beam travels.

The line L can be represented uniquely by the parameters ρ and φ , where φ measures the counterclockwise angle of the line from the vertical, and ρ measures the distance of the line from the origin of the (x, y) plane. Thus, we can use the above formula to define a transform which maps a function $\mu(x, y)$ to a function $g(\rho, \varphi)$, where $g(\rho, \varphi)$ is the line integral of $\mu(x, y)$ over the line defined by ρ and φ . This transform is known as the Radon transform and denoted by R so the Radon transform of $\mu(x, y)$ at the angle φ is the line integral of μ parallel to the y axis:

$$R_\varphi(x') = \int_{-\infty}^{+\infty} \mu(x' \cos \varphi - y' \sin \varphi, x' \sin \varphi + y' \cos \varphi) dy'; \quad (2)$$

$$\begin{bmatrix} x' \\ y' \end{bmatrix} = \begin{bmatrix} \cos \varphi & \sin \varphi \\ -\sin \varphi & \cos \varphi \end{bmatrix} \begin{bmatrix} x \\ y \end{bmatrix}. \quad (3)$$

The function $R_\varphi(x')$ is often referred to as a sinogram because the Radon transform of an off-center point source is a sinusoid and all of the points composing the sample produce a so called sinogram matrix.

Finally, acquired sinograms should be reconstructed to find $\mu(x, y)$ given knowledge of $R_\varphi(x')$, therefore the Filter Back Projection algorithm is used to reconstruct from the measured projections by the filtered back projection method to bring about the inverse Radon transformation. The FBP algorithm begins by filtering the Radon transform data. There are many filters which can be used in our experiments; we used the Ramachandran & Lakshminarayanan (Ram-Lak) filter to remove some of the high-frequency components that are often fraught with noise [13–15].

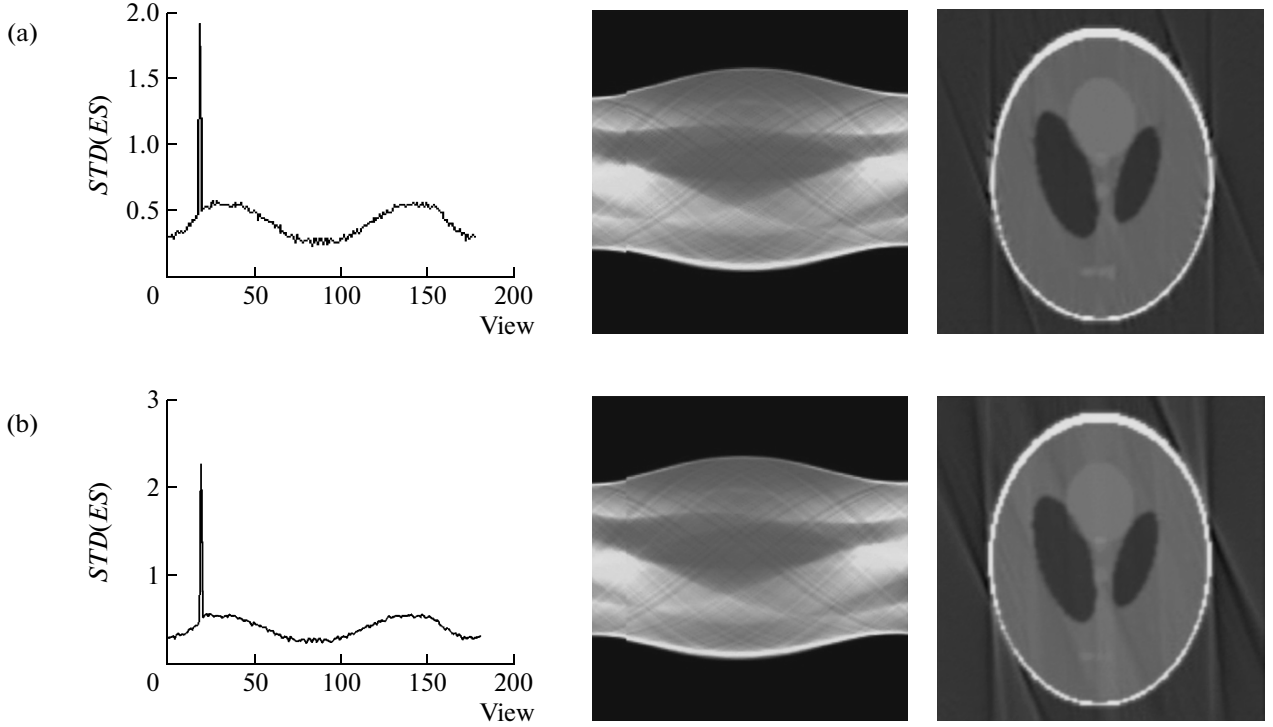


Fig. 3. Left-to-right – STD-errors, sinogram and reconstructed image with changes of (a) axial and (b) rotational in Shepp-Logan phantom.

2.2. Detection of artifacts due to motion in sinogram

For real-time detection of errors due to phantom motion a program was written for extracting the sinogram from the acquired data.

Sinogram is a sinusoidal continuous function. We assume that the variation of sinogram with respect to the view angle is less than the data noise, therefore any deviation from normal distribution of sinogram is considered as a discontinuity which represents the error due to phantom motion as shown below:

$$ES(i, j) = |S(i, j+1) - S(i, j)|, \quad (4)$$

$$i = 1, \dots, n; \quad j = 1, \dots, m-1.$$

Here $ES(i, j)$ is the difference between two successive view columns ($j+1$ -th and j -th) in sinogram matrix $S(i, j)$ (Fig. 1). The standard deviations (STD) of measured errors are calculated by the following equation

$$D(j) = \sqrt{\frac{1}{n} \sum_{i=1}^n [ES(i, j)]^2}. \quad (5)$$

$D(j)$, dislocation parameter represents error due to phantom motion which by drawing standard deviation of errors, any phantom motion can be detected.

It should be noted that the number of $\Delta\theta$ and Δr are views (m) and positions (n) respectively, thus positions \times views ($n \times m$) are called projections [16].

2.3. RMSE

For quantification of the acquired results from experiment and comparing of the effect of phantom dislocation is used the root mean square error that the mathematical formulation is:

$$RMSE = \sqrt{\frac{\sum_{i=1}^N (\mu_{true, i} - \mu_{recon, i})^2}{N^2}}. \quad (6)$$

Where $\mu_{true, i}$ and $\mu_{recon, i}$ are true and reconstructed attenuation mean values at pixel i and N is the total number of pixels [17].

The procedure described can be used for relative comparison of reconstructions of the same object.

3. EXPERIMENTAL SET-UP

A single-source – single-detector gamma computed tomography (CT) scanner system was used in this study. In this system a NaI(Tl) detector 50.8 mm in diameter was located opposite to the center of the ^{137}Cs

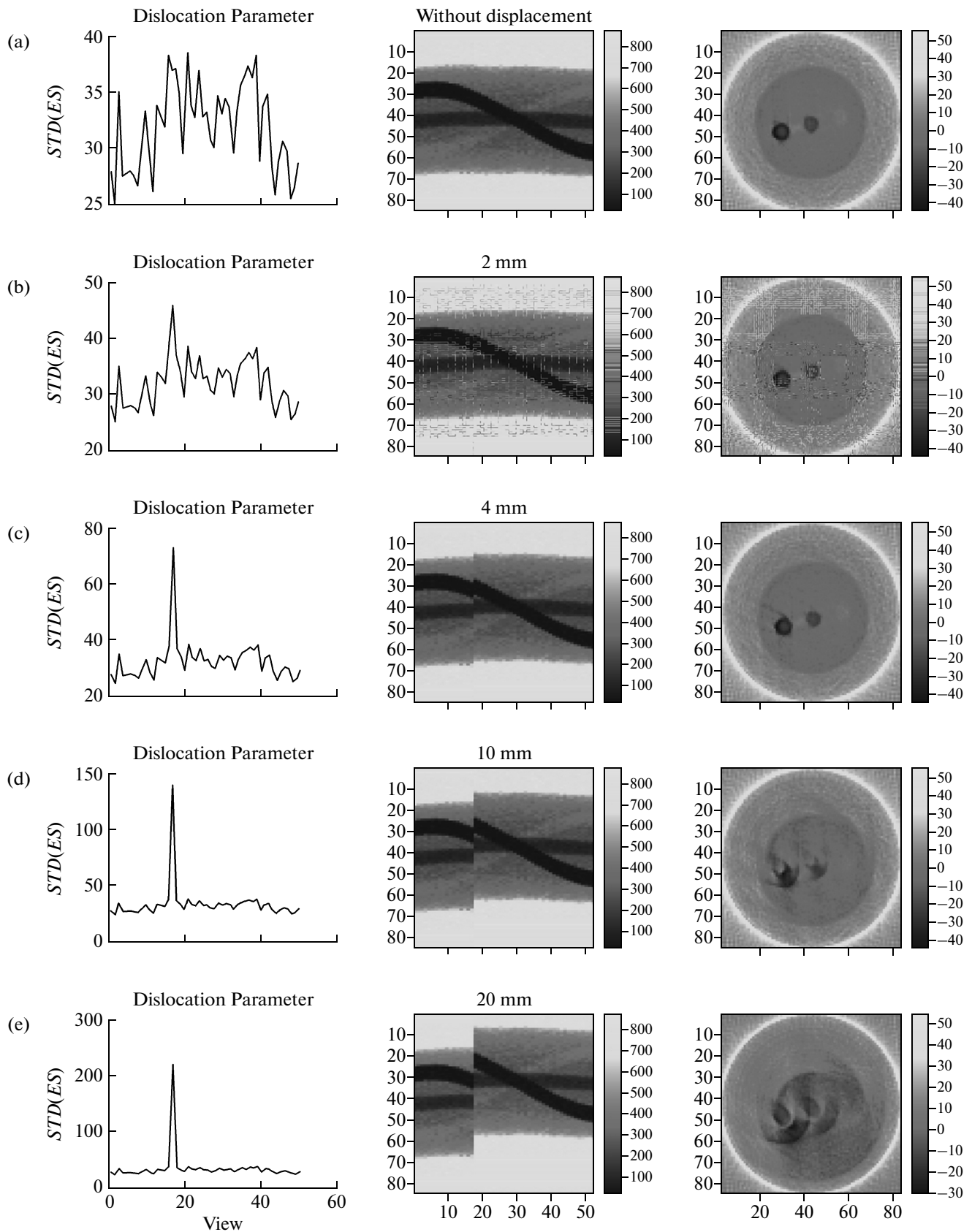


Fig. 4. Left-to-right – STD-errors, sinogram and reconstructed image from polyethylene phantom 2D image, mercury, iron, air holes due to different axial and rotational motion: (a) reconstructed image, sinogram and STD errors without dislocation; (b–e) axial motion with distance 2, 4, 10, 20 mm respectively; (f–i) rotational motion with angle 3.65° , 7.3° , 21.9° , 40.15° respectively.

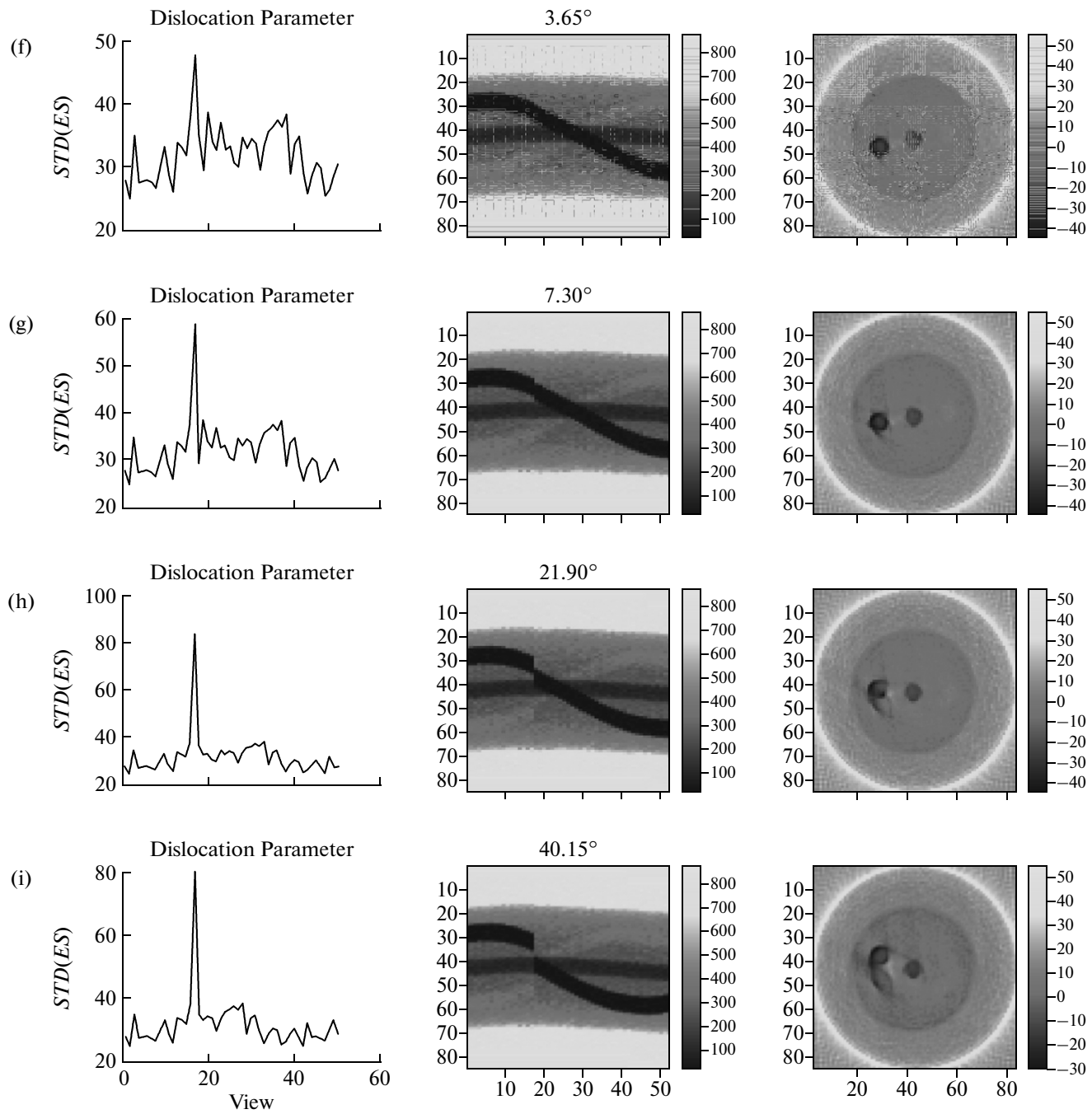


Fig. 4. Contd.

(30 mCi) source at 550 mm distance, where the detector and the source were aligned by a point semiconductor laser.

A polyethylene phantom ($0.93 \text{ g} \cdot \text{cm}^{-3}$) is used to determine the 2D-imaging quality of the designed CT system. The phantom is made as cylinder (100 mm in diameter) on which 3 holes of 15 mm in diameter are drilled. The holes are filled with substances having ex-

panded range of density as mercury ($13.53 \text{ g} \cdot \text{cm}^{-3}$), iron ($7.874 \text{ g} \cdot \text{cm}^{-3}$) and air ($1.184 \text{ mg} \cdot \text{cm}^{-3}$).

The position of phantom is defined by three motors that the phantom was rotated by steps $\Delta\theta = 3.65^\circ$ and moved in the direction of r with $\Delta r = 2 \text{ mm}$. The CT scans are taken out by scanning 180° to collect attenuation beams. There are 4386 projections for producing of image and time of each projection is selected to

RMSE for different axial and rotational motion

Displacement	RMSE, 10^{-4}	Fig. 4
Axial, mm		
2	54	(b)
4	88	(c)
10	191	(d)
20	280	(e)
Rotational, degree		
3.65	23	(f)
7.30	37	(g)
21.90	69	(h)
40.15	94	(i)

be 3 s that the axial and rotational motions were performed after 17th view, separately (Fig. 2).

Nuclear electronic system consists of a NaI(Tl) ($2 \times 2''$, 905-3 model, Eberline company), and a specialized MCA (PSS-1, NSTRI, Tehran, Iran) consists of pre-amplifier, amplifier, high voltage (HV) and a data acquisition system. In this MCA, the software can simultaneously read positions and steps, control the motors and MCA. After that, the image is reconstructed from the measured projections by the filtered back projection method to bring about the inverse Radon transformation.

4. RESULT AND DISCUSSION

4.1. Simulation

An assessment of the effectiveness of the proposed phantom motion tracking technique was carried with simulation using the Shepp-Logan phantom. In this process, we convert the image to sinogram, and then a change (axial [r] and rotational [θ]) equivalent to one pixel (about 0.7 mm) movement was performed on sinogram. Standard deviation of errors due to such distortion was drawn in Fig. 3a–3b where the peak clearly represents the error. Also reconstructed image from altered sinogram was shown in this figure.

4.2. Experimental

Measurements are made with a source of ^{137}Cs (30 mCi) and with the phantom with 3 holes. The results are represented using reconstructed images consisting of the RMSE quantity and acquired errors due to phantom motion, drawing by standard deviation of errors. In this research, experimental conditions for axial and rotational motion were performed in different study stages. In the first stage, phantom is scanned with no displacement. The corresponding STD errors, sinogram and reconstructed image are given in Fig. 4a.

In second stage, phantom was shifted by some distance after 17 views. Fig. 4b–4e represents the acquired results for various shift distances (2, 4, 10, 20 mm). Similarly, the rotational motion was performed after 17 views (at the end of angle = 58.4°) with different shift angles (3.65°, 7.3°, 21.9°, 40.15°). The STD errors, sinogram and reconstructed images are represented in Fig. 4f–4i. The RMSE of each image is given for different axial and rotational motion to compare the reconstruction quality (Table).

5. CONCLUSION

We develop a new technique to detect motion in our γ -ray CT. An ideal result is shown in our simulation with one pixel (about 0.7 mm) displacement detection. Any artifact due to axial motion more than 2 mm and rotational motion more than 3 degree are detectable with this method in our experiment. In our experimental setup, the accuracy and signal-noise ratio (S/N) was degraded because the mechanical tolerance of this equipment is fairly high. Thus, this method can be applicable to other medical imaging instruments and have better results than ones with lower mechanical tolerance.

Unfortunately, the method works poorly in the case of very small and smooth motion. Of course, by further development of this method, (comparing a view column with all of the previous view columns) we can achieve better results. However, an amount of detectable displacement is finite.

In order to correct the detected motion, the scanning is stopped immediately after detection, the position of object is restored to normal and the process is continued. As a result the acquired image is free of any artifact due to the object motion.

These experimental results also show that the changes of the RMSE quantity for axial motion are higher than rotational motion.

This method is easy to use with no additional software required and it can be generalized to other medical and industrial imaging instruments.

REFERENCES

1. Cunningham, I., Stergiopoulos, S., and Dhanantwari, A., *Organ motion effects in medical CT imaging applications, Advanced signal processing handbook*, USA, Boca Raton: CRC press LLC, 2008.
2. Chen, Q.S., Defrise, M., Deconinck, F. et al., *J. Nucl. Med. Technol.*, 1993, vol. 21, p. 198.
3. Tsui, B.M. W., Segars, W.P., and Laush, D.S., *IEEE Trans. Nucl. Sci.*, 2000, vol. 47, p. 1192.
4. Sarkar, S., Oghabian, M.A., Mohammadi, I. et al., *IEEE Transact Nucl Sci.*, 2007, vol. 54, p. 71.
5. Eisner, R.L., Noever, T., Nowak, D. et al., *J. Nucl. Med.*, 1987, vol. 28, p. 97.
6. Linney, N.C., and Gregson, P.H., *IEEE Transact in Med Imaging.*, 2001, vol. 20, p. 1109.

7. Stergiopoulos, S., *JASA*., 1990, vol. 87, p. 2128.
8. Stergiopoulos, S., *Proc IEEE*., 1988, vol. 86, p. 358.
9. Dhanantwari, A.C., and Stergiopoulos, S. *Med. Phys.*, 2001 vol. 28, vol. 28, p. 1577.
10. Kak, A.C., and Slaney, M., *Principles of Computerized Tomographic Imaging*, USA, IEEE Service Center, 1999.
11. Milanfar, P., *IEEE Trans. Image. Proc.*, 1999, vol. 9, p. 1276.
12. Kim, J., and Jung, S., *Nucl. Engin. Tech.*, 2006, vol. 38, p. 383.
13. Herman, G.T., *Fundamentals of Computerized Tomography: Image Reconstruction from Projections*, Ed. 2, USA, Springer, 2009.
14. Bushberg, J.T., Seibert, A., Leidholdt, E.M., and Boone, J.M., *The Essential Physics of Medical Imaging*, Philadelphia: Lippincott Williams & Wilkins, 2000.
15. Deans, S.R., *The Radon Transform and Some of Its Applications*, NY.: Wiley, 1983.
16. Gholipour Peyvandi, R., Islami Rad, S.Z., Heshmati, R., and Ghannadi Maragheh, M., *Instrum. Exp. Tech.*, 2011, vol. 54, p. 542.
17. IAEA-TECDOC 1589, *Industrial process gamma tomography, final report of a coordinated research project 2003–2007*, Austria, International Atomic Energy Agency, 2008.